



UNIVERSITA' DEGLI STUDI DI NAPOLI FEDERICO II

FACOLTÀ DI FARMACIA
DIPARTIMENTO DI CHIMICA FARMACEUTICA E TOSSICOLOGICA

**DOTTORATO DI RICERCA IN
SCIENZA DEL FARMACO XIX CICLO**

*CHARACTERIZING THE 1,4-DIHYDROPYRIDINES BINDING INTERACTIONS
IN THE L-TYPE Ca^{2+} CHANNEL:
MODEL CONSTRUCTION AND DOCKING CALCULATIONS*

Coordinatore
Chiar.mo Prof. Enrico Abignente

Supervisore
Chiar.mo Prof. Ettore Novellino

Candidato
Dott. Sandro Cosconati

INDEX

Introduction	pag. 1
Computational Methods	pag. 14
Construction of the Human LCC Model	pag. 15
Docking Simulations	pag. 18
Ligand Setup	pag. 19
Protein Setup	pag. 20
Energy Refinement of DHPs/LCC complexes	pag. 21
Results and Discussion	pag. 22
Sequence Alignment Between LCC S5s and S6s with KcsA M1 and M2 Segments	pag. 23
P-Loops Construction	pag. 29
Assembly of the P-Loop Region with the Transmembrane Bundle of LCC	pag. 33
DHPs docking	pag. 38

DHPs Docking on Model A of LCC	pag. 41
DHPs Docking on Model B of LCC	pag. 49
From Antagonist to Agonist DHPs	pag. 53
Conclusions	pag. 58
References	pag. 6

INTRODUCTION

Ca^{2+} channels are transmembrane proteins that, upon membrane depolarization, allow the selective passage of Ca^{2+} ions into excitable cells. By controlling the entry of Ca^{2+} into cells, these proteins have a critical role in a broad range of cellular processes, such as neurotransmitter release, second messenger cascades, cardiac excitation and contraction, and gene regulation supporting learning and memory.¹ The Ca^{2+} channel family contains at least ten members that are distinguished by their structure, subunit composition, location, biophysical properties and pharmacology. According to their electrophysiological and pharmacological properties Ca^{2+} channels are distinguished in N-, L-, T-, P/Q-, and R-type channels.² Among these, the L-Type Ca^{2+} channel (LCC) has been characterized extensively through biochemical approaches. These studies revealed that LCCs are heteromultimeric proteins consisting of a central pore-forming α_1 subunit that expresses the major biophysical, functional and pharmacological properties of the channel. This subunit is associated with a number of auxiliary subunits, $\alpha_2\delta$, β and γ that control channel expression, membrane incorporation, drug binding and gating characteristics of the central unit.³

Like in the structurally homologous K^+ and Na^+ channels,⁴ also the α_1 subunit of LCC is made up by four homologous domains (repeat I-IV) each consisting of six transmembrane α -helical segments (S1-S6). The central pore of the channel is formed by the S6 segment of each subunit and by the extracellular region between S5 and S6 segments (P-loop) that deepens into the pore, forming the extracellular mouth of the channel. Four conserved Glu residues, in the four P-loops, form the so called EEEE locus which act as a selectivity filter for the passage of Ca^{2+} and other divalent ions.⁵

From the pharmacological point of view, LCC represents a realized and ongoing opportunity for drug intervention being target of three different chemical categories of drugs (Fig. 1): 1,4-dihydropyridines (DHPs such as nifedipine), phenylalkylamines (PAAs such as verapamil), and benzothiazepines (BTZs such as diltiazem).⁶

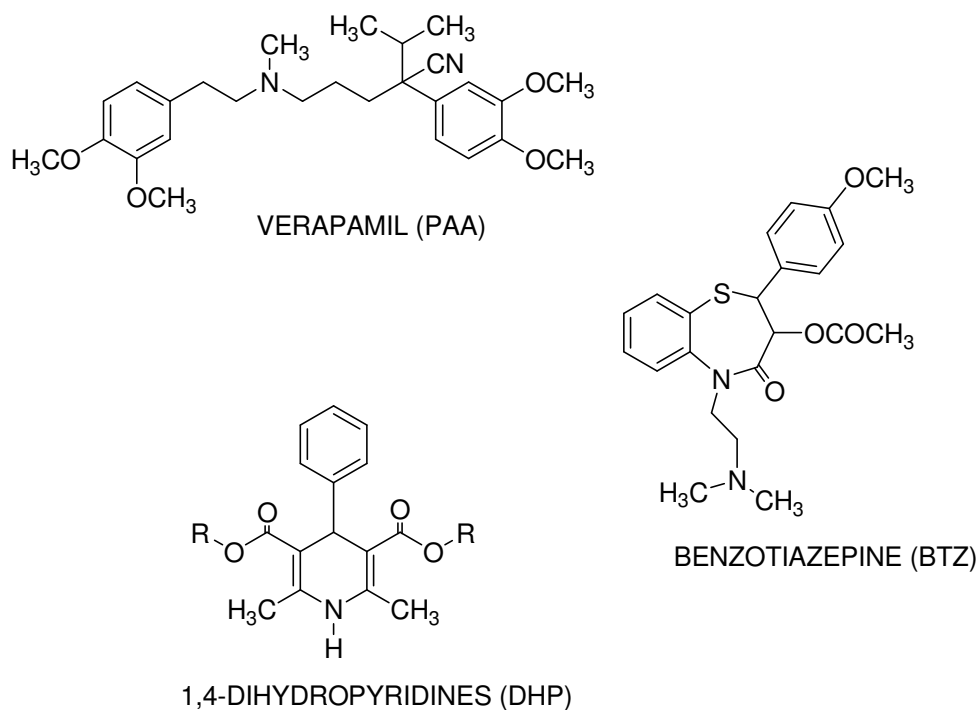


Figure 1. General structures of ligands known to antagonize LCC.

These drugs are used in the treatment of cardiovascular disorders, including hypertension, arrhythmias, angina, and cerebral and peripheral vascular disorders.⁷ While verapamil and diltiazem are the only therapeutically available members of their respective families, DHPs are well represented in a number of second and third-generation agents. The binding sites of all these drugs are positioned beneath the selectivity filter and ligand

binding studies indicate that PAAs, BTZs, and DHPs bind to three separate channel regions that interact allosterically.⁸ Several studies indicate that PAAs reach their binding site from the cytoplasm and are considered to be pore-blocking drugs that block LCC directly by occluding the transmembrane pore through which Ca^{2+} ions move. In contrast, DHPs bind to a single site at which agonists increase Ca^{2+} channel activity and antagonists reduce it, so they cannot bind in a manner that blocks the pore. Therefore, DHP antagonists appear to block the pore indirectly by stabilizing a channel closed state with a single Ca^{2+} ion bound in a blocking position in the pore.⁹ Despite the large body of evidences regarding the specific residues involved in the binding of these drugs together with the extensive structure-activity relationships (SARs) data on the different compounds, it is still not absolutely clear how these molecules actually bind to LCC and which are the main ligand-LCC interactions responsible for the high affinity to the channel. Since the three-dimensional (3D) structure of LCC is not available, different theoretical models of this channel were reported and in some of them the binding pose of LCC-antagonist was also described. Most precisely, in pioneering studies by Lipkind and Fozzard¹⁰ and Zhorov and co-workers¹¹

the binding pose of DHPs in LCC was obtained by docking a limited set of ligands into their putative binding site. It is worth noting that in the first study a manual docking procedure was adopted and their reliability could be influenced by personal biases and/or ambiguous experimental data. In the second study by Zhorov and co-workers nifedipine was docked using a Monte Carlo minimization (MCM) method. Indeed, also the small number of docked ligands might impede to verify the consistency of the predicted ligand-protein complexes with the wide amount of experimental data.

Therefore in the present study, starting from the above cited studies of Zhorov and co-workers, a model of the central pore region of the human LCC α_{1c} subunit (Ca_v1.2) was constructed to get major insights on the specific interactions between DHPs antagonist and LCC. Then, the obtained 3D structure of the LCC inner pore was used for automated docking calculations of several DHPs bearing different substituents on the 4-aryl ring and on the esters in position 3 and 5 of the DHP ring. As regards the construction of the pore region of LCC, the X-ray 3.20 Å crystal structure of the bacterial K⁺ channel KcsA determined by Doyle et al was used.¹² In this

work all the previous assumptions about the topology of the ion-channel superfamily were confirmed, in fact, like Ca^{2+} channels, KcsA is made up by four subunits each consisting of only two transmembrane α -helical segments (M1 and M2) rather than six, connected by an extracellular loop (Fig. 2).

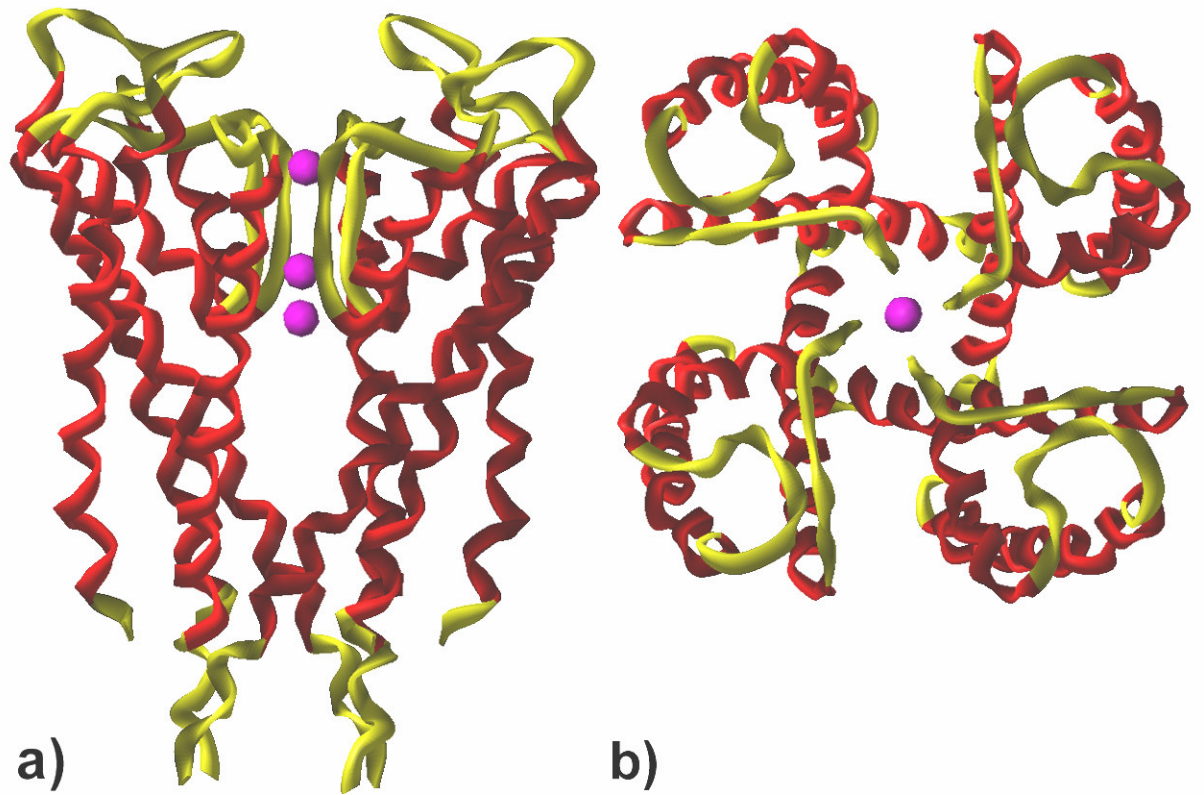


Figure 2. Ribbon representation of the 3D crystal structure of KcsA.

Unlike LCC, KcsA is a homotetrameric rather than an eteromeric protein. Nevertheless, it was suggested that this KcsA architecture also describes the pore of Na⁺ and Ca²⁺ channels and it could be speculated that KcsA is an evolutionary predecessor of the six-transmembrane segment ion channels.¹³ Thus, it seems reasonable to choose the 3D structure of KcsA as a starting point for the construction of both the transmembrane and P-loop regions of LCC. More recently, Jiang et al. have determined the 3D structure of the open Ca²⁺-activated K⁺ channel MthK.¹⁴ This structure is almost identical to KcsA apart from a hinge region in the M2 segment made of some glycine residues critical in the activation of this channel. Considering that voltage-opened Ca²⁺ channels have larger residues in the corresponding positions and the above cited turning point would not be feasible, the construction of the transmembrane portion of LCC using the MthK as a template does not seem viable.

The constructed model of LCC was then used to dock different DHPs. The ligand-channel complexes were predicted using an automated docking software, AutoDock.¹⁵ The choice of this software was dictated by its high efficiency in predicting the real experimentally found ligands binding

conformations.¹⁶ This program was used to dock eight different antagonists and one agonist DHP featuring molecular diversity (Fig. 4). In such a study, in order to distinguish between the two sides of DHPs, as suggested by Goldman et al. the preferred conformation of this ring will be regarded as a flattered boat with C4 as the bow, the axial aryl ring as the bowsprit and the N1 atom as the stern (Fig. 3a). The two sides of the DHP ring will be then referred as the port side (left) and the starboard side (right) (Figure 3b).¹⁷

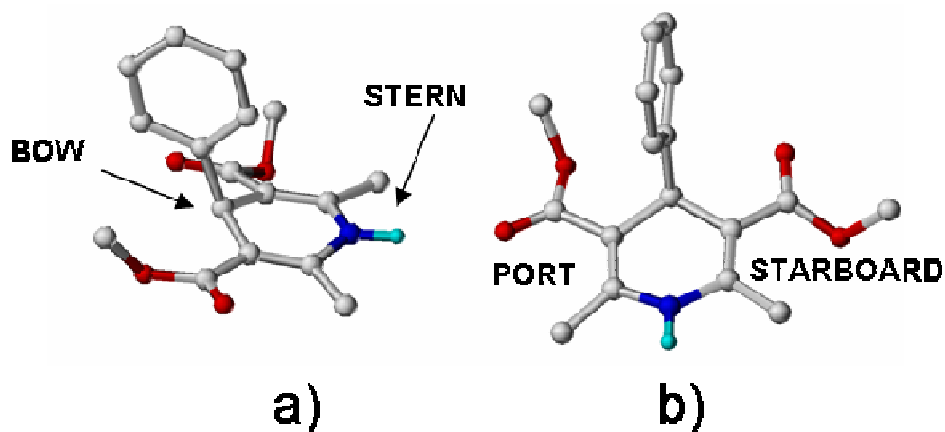


Figure 3. General structure of DHP drugs with the adopted nomenclature highlighted.

The binding mode of nifedipine¹⁸ was inspected as it is the most structurally representative DHPs that was first introduced as an antihypertensive and antianginal agent 30 years ago. (S)-nitrendipine¹⁹ and lacidipine²⁰ were docked so to evaluate if the presence of the nitro group in *ortho* position or the presence of the large α - β unsaturated ester system on the aryl ring could be easily located in the LCC model. DHPs with unsymmetrical ester substitution are generally more active pharmacologically than those with symmetrical substitution,^{6,17} therefore, to detect the reasons behind this behaviour (S)-isradipine,²¹ (R)-amlodipine,²² (S,S)-furnidipine²³ and (S,S)-benidipine²⁴ were also docked. In particular, docking of (S)-isradipine was also performed with the aim of evaluating the influence of the benzoxadiazole ring in position 4 on ligand binding. The importance of the charged alkyl substituents in position 2 was inspected by docking (R)-amlodipine, while (S,S)-furnidipine and (S,S)-benidipine were docked in order to assess the role on binding of large lipophilic substituents on the port side ester group. Some DHP display a peculiar pharmacological behaviour when the absolute configuration of their chiral centre at position 4 is changed

from the (*R*)-configuration to the (*S*)-one. In fact, while the first one has antagonist properties towards LCC the latter is an activator of this channel. This is the case of Bay K 8644 and for these reasons both isomers of this ligands were also docked. Figure 4 reports the structures of the inspected compounds.

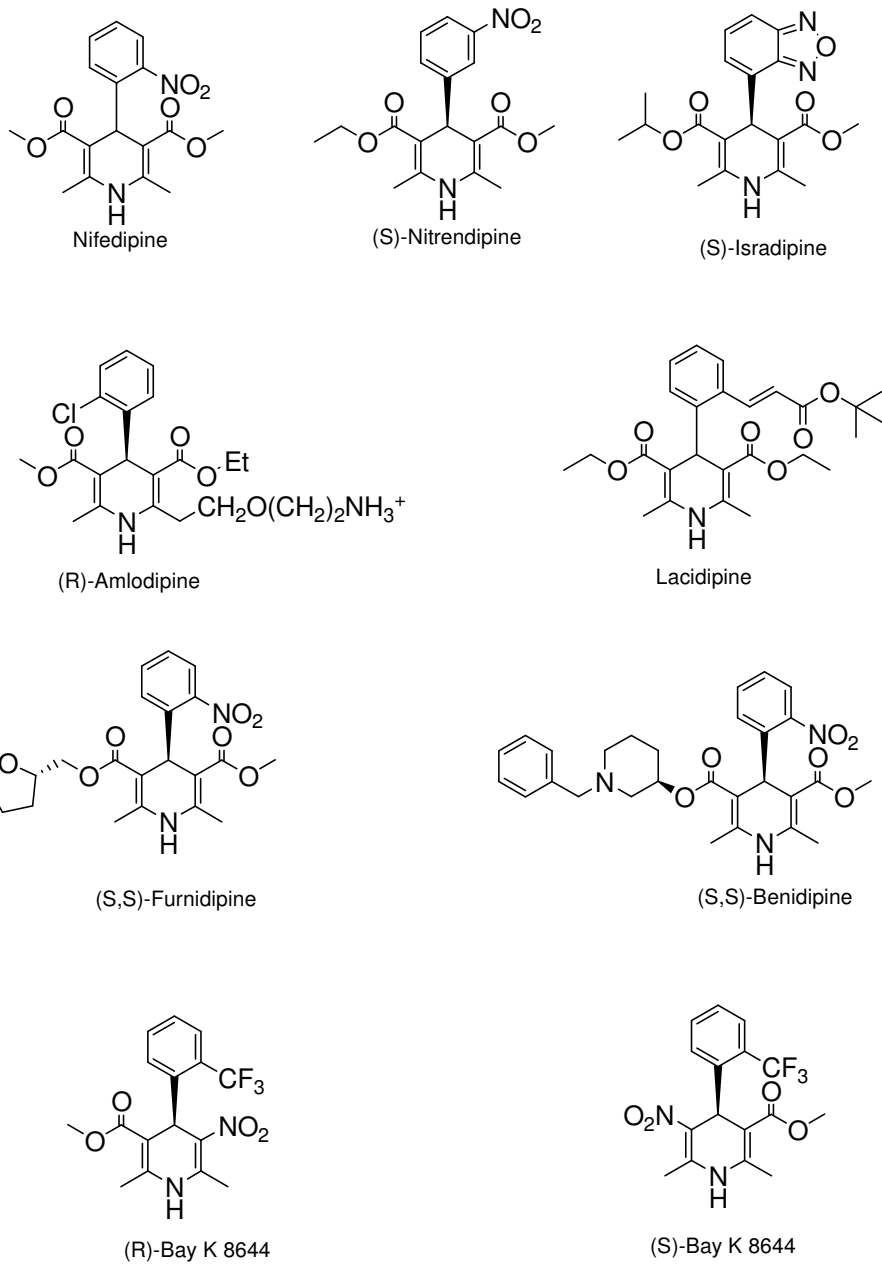


Figure 4. Structures of the investigated ligands

The employment of automated docking procedure allowed to determine at atomic resolution the receptor-bound conformations of several DHPs endowed of antagonist activity towards LCC. Indeed, the consistency of the predicted binding pose of these ligands in LCC with SARs and mutagenesis data confirms the feasibility of the calculated binding modes. In this respect, the present study gives for the first time a detailed description of the main interactions between LCC and DHPs obtained with the employment of an automated docking algorithm.

COMPUTATIONAL METHODS

Molecular modeling and graphics manipulations were performed using the SYBYL 7.2²⁵ and InsightII²⁶ software packages, running on a Silicon Graphics Tezro workstation equipped with four 700 MHz R16000 processors. Energy minimizations and MD simulations were realized by employing the module Discover3²⁶ within InsightII, selecting the consistence-valence force field (CVFF).²⁷

Construction of the Human LCC Model. The structural model of the human LCC was built using the recently reported 3.20 Å crystal structure of KcsA¹² (PDB entry code 1BL8) as a structural template. The sequence of human LCC pore region α_{1c} subunit (Ca_v1.2, CAC1C_HUMAN) was retrieved from the SWISS-PROT database²⁸ and aligned as described in the Results and Discussion section (Figure 5). The construction of the transmembrane region of the two alternative models (Model A and B) was achieved with the employment of the HOMOLOGY module within InsightII which was also used to check the consistence of bond distances, bond angles, and torsion angles with proteins standard values. After construction of the

transmembrane region of both Model A and B, the whole structures were energetically minimized using the Discover3²⁶ module of the InsightII suite of programs with 5000 steps of a steepest descent minimization reaching a convergence of 10.0 kcal mol⁻¹ Å⁻¹, followed by 3000 steps of conjugate gradient minimization reaching a final convergence of 0.01 kcal mol⁻¹ Å⁻¹ to eliminate any residual geometrical strain, keeping the backbone atoms fixed. The same procedure was also followed for the construction of the P-loop region of LCC (for sequence alignment see Figure 5).

After construction of both P-loop and transmembrane regions for Model A and B the extracellular and transmembrane portion were assembled using the a protein-protein docking program. ZDOCK²⁹ software was used for rigid-body docking of the P-loop on the transmembrane region of LCC. This docking method is based on the FFT correlation approach³⁰ that systematically evaluates a simple grid-based scoring function over billions of relative orientations of the two proteins. ZDOCK scoring function includes a combination of shape complementarity, Coulombic electrostatics, and desolvation free energy based on the Zhang et al.³¹ atomic contact potential. As default, ZDOCK retains 2000 structures. FFT-based tools are used to

rapidly generate a large number of protein-protein conformations with good shape complementarity and with relatively favourable electrostatics and desolvation values. The top 20,000 structures were retained and ranked by the automated Cluspro web server (<http://nrc.bu.edu/cluster>).³² The 30 different models achieved from the docking run were then analyzed according to the arrangement of the P-loop region on the transmembrane bundle. The best solutions for Model A and B were then used as initial structure for the subsequent molecular dynamics (MD) simulation. The selectivity-filter area of LCC contains eight negatively charged residues which are not counterbalanced by any positively charged one. Since Ca^{2+} ions should be the ones that are more present in this channel, four Ca^{2+} ions were added to the P-loop region so to interact with the above cited acidic residues. MD calculation was then begun with an initial and equilibration stage (500 ps), followed by a production run (1000 ps). In the equilibration stage, energy minimization of the protein side chains were achieved employing 3000 steps of steepest descent. Subsequently, the system was heated gradually starting from 10 to 310 K in 1 ps steps. The system was then equilibrated with temperature bath coupling (310 K) applying a

tethering force on the backbone starting from 100 kcal/Å⁻² and decreasing to 20 kcal/Å⁻². A cutoff of 18 Å was used for nonbonded interactions. Coordinates and energies of the production run were saved every 10 ps yielding 100 structures. The average structure was calculated over the 100 structures of the production run and was energy-minimized using 3000 steps of a steepest descent minimization keeping the backbone atoms constrained. The stereochemical quality of the final structure was analyzed using the program PROCHECK.³³

Docking Simulations. Docking of nifedipine, (*S*)-nitrendipine, (*S*)-isradipine, (*R*)-amlodipine, lacidipine, (*S,S*)-furnidipine and (*S,S*)-benidipine was performed with version 3.05 of the AutoDock software package.¹⁵ It combines a rapid energy evaluation through pre-calculated grids of affinity potentials with a variety of search algorithms to find suitable binding positions for a ligand on a given protein. While the protein is required to be rigid, the program allows torsional flexibility in the ligand. Docking to LCC was carried out using the empirical free energy function and the Lamarckian genetic algorithm, applying a standard protocol, with an initial population of

50 randomly placed individuals, a maximum number of 1.5×10^6 energy evaluations, a mutation rate of 0.02, a cross-over rate of 0.80, and an elitism value of 1. Proportional selection was used, where the average of the worst energy was calculated over a window of the previous 10 generations. For the local search, the so-called pseudo-Solis and Wets algorithm was applied using a maximum of 300 iterations per local search. The probability of performing the local search on an individual in the population was 0.06, and the maximum number of consecutive successes or failures before doubling or halving the local search step size was 4. 50 independent docking runs were carried out for each ligand. Results differing by less than 1.5 Å in positional rmsd were clustered together and represented by the result with the most favourable free energy of binding.

Ligand Setup. The core structures of all ligands were retrieved from the Cambridge Structural Database (CSD)³⁴ and modified using standard bond lengths and bond angles of the SYBYL fragment library. Geometry optimizations were realized with the SYBYL/MAXIMIN2 minimizer by

applying the BFGS (Broyden, Fletcher, Goldfarb, and Shannon) algorithm³⁵ and setting a rmsd gradient of the forces acting on each atom of 0.05 kcal/mol Å as the convergence criterion. Atomic charges were assigned using the Gasteiger-Marsili formalism,³⁶ that is the type of atomic charges used in calibrating the AutoDock empirical free energy function. Finally, all compounds were set up for docking with the help of AutoTors, the main purpose of which is to define the torsional degrees of freedom to be considered during the docking process. The number of flexible torsions defined for each ligand is two for nifedipine, three for (*S*)-nitrendipine (*S*)-isradipine (*R*)- and (*S*)-Bay K 8644, seven for (*R*)-amlodipine, six for lacidipine, four for (*S,S*)-furnidipine, five for (*S,S*)-benidipine.

Protein Setup. Both Model A and B of LCC were set up for docking as follows: only polar hydrogens were added using the biopolymers module of the SYBYL program, (Arg, Lys, Glu, and Asp residues were considered ionized, while all His were considered neutral by default), and Kollman united-atom partial charges were assigned. Solvation parameters were added to the final protein file using the addsol utility of AutoDock. The grid maps

representing the proteins in the actual docking process were calculated with AutoGrid. The grids (one for each atom type in the ligand, plus one for electrostatic interactions) were chosen to be sufficiently large to include not only the active site but also significant portions of the surrounding surface. The dimensions of the grids were thus $60 \text{ \AA} \times 60 \text{ \AA} \times 60 \text{ \AA}$, with a spacing of 0.375 \AA between the grid points.

Energy Refinement of DHPs/LCC complexes. Refinement of the predicted DHP/LCC complexes was achieved through energy minimizations using the Discover3 module of InsightII. These geometric optimizations included 5000 steps of a steepest descent minimization reaching a convergence of $10.0 \text{ kcal mol}^{-1} \text{ \AA}^{-1}$, followed by 3000 steps of conjugate gradient minimization reaching a final convergence of $0.01 \text{ kcal mol}^{-1} \text{ \AA}^{-1}$, keeping the backbone atoms fixed and LCC side-chains and the ligand free to move.

RESULTS AND DISCUSSION

Sequence Alignment Between LCC S5s and S6s with KcsA M1 and M2 Segments

When modeling a protein on a template structure, sequence alignment is the most important stage. As regards the construction of a model of the central pore of LCC, this task becomes really challenging due to the low sequence identity between KcsA and LCC. In consonance with what suggested by other authors,^{10,11} the sequence of the LCC central pore with the sequence of KcsA was aligned considering the mutagenesis data present in literature on Ca²⁺-antagonists. Therefore, starting from the assumption that ligand-sensing residues are supposed to be located in the same region, the best alignment would be the one that maximizes the propinquity of such residues.

In order to detect the interacting residues for dihydropyridines (DHP), phenylalkylamines (PAA), benzothiazepines (BTZ) several experimental studies (photoaffinity labelling, construction of chimeric channels) were reported in literature. This data unambiguously demonstrate that IIS6 IVS6 and IIS5 transmembrane segments interact with the antagonists.³⁷⁻³⁹ Table 1

summarizes results of mutations in LCC segments IVS6, IIIS6, IIIS5 and IIIP on binding of a DHP-antagonists (different DHP antagonists were used for these reported inspections).

Table 1. Effect on antagonist binding of mutagenesis experiments on LCC.

Segment	WT Residue	WT Residue in Human LCC	Mutant Residue	Mutant IC ₅₀ /WT IC ₅₀	Ref.
IVS6	Tyr1463	Tyr1508	Ala	6.1	39
	Met1464	Met1509	Ala	1.6	39
	Ile1471	Ile1516	Ala	2.7	39
IIIS6	Tyr1152	Tyr1169	Ala	25	40
			Phe	12.4	40
	Ile1153	Ile1170	Ala	6.2	40
	Ile1156	Ile1173	Ala	17	40
	Met1160	Met1177	Ala	3.5	40
	Met1161	Met1178	Ala	9.6	40
IIIS5	Thr1056	Thr1066	Tyr	>1000	37, 42
			Ala	1	37,42
	Gln1060	Gln1070	Met	29.4	37, 42
IIIP	Phe1112	Phe1128	Ala	5.1	9, 49
	Ser1115	Ser1131	Ala	39.4	9, 49

From mutagenesis data, it has been clarified that three amino acid residues are critical for the interaction with DHPs in the IVS6 segment Tyr1508, Met1509 and Ile1516 and it is likely that these amino acids face the pore.⁴⁰ As concerns the IIS6 segment several residues are responsible for the binding with DHPs: Tyr1169, Ile1170, Ile1173, Met1177 and Met1178.⁴¹ Taken together, all this data indicate that DHPs interact with the LCC by binding between the IIS6 and IVS6 helices.⁴² Mutagenesis data also indicated that in IIS5 residues Thr1066 and Gln1070 are important for binding of DHPs.^{38,43}

With the aim of building an accurate model of the LCC, as suggested by Lipkind and Fozzard, two different sequence alignments of the transmembrane segments with KcsA can be hypothesized.¹⁰ As regards the IVS6 segment, it has been proposed to align the M2 Trp87 residue of KcsA with the hydrophobic residue Phe1499. This alignment allows Tyr1508 to face the pore in accordance with mutagenesis data that demonstrate its important role in binding with the DHPs, and locates Ile1173 to form the bottom of the putative binding site.^{10,11}

For the alignment of IIS6 segment to M2 of KcsA two possibilities were given in the first one Glu1161 is aligned with Trp87 of KcsA. This alignment allows placing Tyr1169, Ile1170, Ile1173 Met1177 and Met1178 at the IIS6-IVS6 interface. Another sequence alignment can be taken into account in which the hydrophobic residue Val1160 is aligned with Trp87; this option places both the important residues of IVS6 Tyr1169 and Tyr1508 at the same level. It is worth noting that with this alignment, residues Ile1170 and Met178, which mutagenesis data indicate as DHPs interacting residues, are placed outside the pore. Indeed, the preference for one of the two proposed alignments of the segment IIS6 of LCC with M2 of KcsA cannot be unambiguously determined, hence, two different candidate models were built for both alignments of IIS6. This alternative model will be referred as follows: Model A in which Glu1161 is aligned with Trp87of KcsA, Model B in which Val1160 of LCC is aligned with Trp87 of KcsA. The predilection for one of the two candidates will be ultimately given on the basis of the consistency of docking results of DHPs conducted on both models with SARs and mutagenesis data.

Less information are available for segments IS6 and IIS6 so it was suggested to align the hydrophobic Trp380 (IS6) and Leu728 (IIS6) with Trp87 of KcsA.¹⁰ A Gly residue at the C-terminus of the LCC S5 segments is really conserved, thus they were all aligned so as to allow this residues to coincide with the identical Gly43 of KcsA. Moreover, with this alignment, Thr1066 and Gln1070, which are important for the interaction with DHPs,⁴³ are placed in vicinity of the putative binding site of DHPs, corresponding to the position of Thr32 and Leu36, respectively. Figure 5 reports the proposed alignment.

KcsA

M1 AGAATVLLVIVLLAGSYLA 47

CAC1C_HUMAN

IS5 IALLVLFVIIYAIIGLELF 290

IIS5 LLLLFLFIIIFSLIGMQLF 673

IIIS5 VIVTLLQFMFACIGVQLF 1071

IVS5 ALLIVMLFFIYAVIGMQVF 1430

KcsA

P ITYPRALWWSVETATTVGYGD 80

CAC1C_HUMAN

IP DNFAFAMLTVFQCITMEGWTD 367

IIP DNFPQSLTTFVQILTGEDWNS 710

IIIP DNVLAAMMALFTVSTFEGWPE 1138

IVP QTFPQAVLLLLFRCATGEAWQE 1468

KcsA

M2 WGRCVAVVVMVAGITSFGLVTAALAT 112

CAC1C_HUMAN

IS6 WPWIYFVTLIIIGSFFVLNLVVGVS 405

IIS6 LVCIYFIILFICGNYILLNVFLAIAV 753

IIIS6 (MODEL A) VEISIFFIIYIIIIIAFMMNIFVGFV 1185

IIIS6 (MODEL B) EISIFFIIYIIIIIAFMMNIFVGFVI 1186

IVS6 FAVFYFISFYMLCAFLIINLFVAVIM 1524

Figure 5. Pairwise alignment of CAC1C_HUMAN and KcsA sequences.

The conserved key residues used to align the sequences are shown in red boxes. Residues reported to affect DHPs antagonist binding and underscored and highlighted in bold

P-Loops Construction

The extracellular region between M1 and M2 segments of KcsA and MthK deepens into the pore, forming a narrow region of 12Å, lined by the main chain carbonyl oxygens of the sequence TXGYG acting as selectivity filter allowing only the passage of K⁺ ions.^{12,14} On the other hand, in LCC the side chains of highly conserved Glu residues form a ring called the EEEE locus that act as a selectivity filter for the passage of Ca²⁺ ions. Thus, in KcsA permeating cations interact with the backbone carbonyl groups of the residues in the selectivity-filter region, while in other P-loop channels ions should interact with the side chains of selectivity-filter residues. Hence, it was argued that the selectivity filters controlling peculiar features of K⁺, Na⁺, and Ca²⁺ channels should have different structures.¹⁰ For these reasons, several models of LCC were proposed in which KcsA was used as templates only for general folding.⁴⁴ In contrast, in 2005 Zhorov and co-worker proposed a model of Na⁺ channel P-loop region, using MthK coordinates in which the P-Loop region shares an almost identical folding of the correspondent portion in KcsA.⁴⁵ These studies clearly demonstrated that

experimentally available data on the Na⁺ channel selectivity-filter region could be explained without great modification of the X-ray template of the P-loop region in MthK. Most precisely, it was demonstrated that pharmacological and electrophysiological features of the Na⁺ channel could be reproduced in the model through minor adjustments of the channel template in the selectivity-filter region without displacing the entire P-loops. This suggests that the P-loop region of voltage gated Na⁺ channels, of KcsA and of MthK have similar 3D structures. Moreover, the same considerations could be raised for the P-loop region of LCC. In fact, several experimental evidences indicate that the substitution of selectivity filter residues Lys1422 and Ala1714 in the Na⁺ channel (forming the DEKA locus) with Glu (DEEE) provides Ca²⁺-selectivity to the channel.⁴⁶ In addition, this channel featured some peculiar pore behaviour of native Ca²⁺ channels, such as permeation by Na⁺ in the absence of Ca²⁺.⁴⁷ Furthermore, the double LCC mutant, E1086K/E1387A (human L-type Cav1.2), (EEKA locus) led to a channel with pore characteristics analogous to those of Na⁺.⁴⁸

Taken together, these considerations support the use of the 3D coordinates of KcsA P-loop region as a template for the construction of the LCC P-

Loops. It is worth noting that it does not seem viable to model the entire extracellular portion between the S5 and the S6 helices. Actually, these large loops have different lengths among the four subunits and the little experimental data are not sufficient to model the whole region. Possibly, the portion between the S5 segments and P-Loops is involved in binding of large peptide toxins, but most of drugs of medicinal interest bind at other sites.³⁷⁻⁴³ As previously reported, several mutagenesis data suggest that DHPs binding site is located between the IIS6 and IVS6 helices then, ignoring the extracellular portion between P-loops and S5 segment is unlikely to affect results of the present molecular modeling study, consequently solely the LCC extracellular pore region was modelled.

In order to model the P-loop portion of LCC it was essential to choose a proper sequence alignment between LCC and KcsA channels. In this study the alignment reported by Tikhonov et al.⁴⁵ and Yamaguchi et al.⁴⁶ was used. This alignment places Phe1128, Ser1131 and Phe1133 present in P-loop repeat III to form part of the putative binding pocket of DHPs. Interestingly, this is in accordance with mutagenesis data indicating the important role of such residues in the interaction with these ligands.^{9,50}

It is worth noting that this alignment places all the Glu residues of the selectivity filters at the same level even though several authors suggested an asymmetrical alignment so to give explanation for the presence of accessory Ca^{2+} binding sites. On the other hand, pairwise replacement of the four glutamates excluded the hypothesis of two high affinity Ca^{2+} binding sites therefore it was concluded that the Glu residues had to be located at the same level forming a single selectivity filter ring.⁵⁰ In order to get a model of the LCC pore region each residue of KcsA channel pore region model was systematically mutated into the correspondent ones of LCC according to the above reported alignment. Afterwards, the structure was energetically minimized with the aim of removing all sterically unfavourable contacts.

Assembly of the P-Loop Region with the Transmembrane Bundle of LCC

After construction of LCC pore region, this portion was adapted on the model of the transmembrane bundle of Ca^{2+} channel. Noticeably, the extracellular region of LCC cannot be placed in the same position of KcsA and MthK P-loops. In fact, while the highly conserved residue Gly99 in segment M2 of KcsA is in close vicinity of the P-loop Ala73,¹² in the present model Gly99 is replaced by Ile1172 of LCC that, with its bulkier side-chain, prevents a similar adjustment in LCC. Therefore, the pore region of LCC must be sited higher, closer to the extracellular side of the membrane.¹⁰

In absence of detailed information at atomic level of the specific interactions between the P-loop region and the transmembrane bundle of LCC accurate and predictive protein-protein docking methods might provide substantial knowledge about the 3D structure of this channel. To make progress in characterizing the interactions between the transmembrane and the outer region of the channel a model of LCC pore region was generated performing a rigid-body protein-protein docking of the structure of the P-

loop region on both Model A and B of the transmembrane bundle using the program ZDOCK.²⁹ The choice of this docking software implemented in ClusPro server was supported by the outstanding results achieved through their employment in the CAPRI experiments where it has shown to be a fast and reliable predictor of protein-protein complexes, provided that the complex does not undergo a significant structural transformation upon binding.⁵¹ 30 different models were achieved from the docking run and analyzed according to the arrangement of the P-loop region on the transmembrane bundle. In both docking runs of the P-loop structure on the two models (A and B) of the transmembrane region, the top ranking structure generated by ZDOCK placed the outer region in a reasonable position, in fact, the P-loop portion of each repeat was in both cases adjusted in the crevice formed by S5 segment of the same repeat and the S6 segment of the adjacent one. All other models generated by ZDOCK were discarded due to the implausible binding interactions between the two portions.

With the intention of building a realistic model of LCC, the generated models for candidates A and B were also analyzed to see if they were in accordance with experimental data. Actually, mutagenesis experiments allow

to infer that the selectivity filter (EEEE locus) is in close proximity of Tyr1508.³⁷ In fact, DHP binding is not affected by mutation of residues above Tyr1508, thus suggesting that this portion might be in close contact with the pore region.^{37,38} Moreover, when mutating this residue to Ala, the reversal potential of the channel is altered by 15mV and permeation of N-methyl-D-glucamine is increased suggesting that this residue is near the selectivity filter.³⁷

A comparison of the amino acid sequences of the P-loop region of different LCCs reveals that all DHP-sensitive channels have a Phe1113 adjacent to Glu1114 residue of the selectivity filter in the P-loop region of repeat III, while all DHP-insensitive channels have a Gly at this position.⁹ From mutagenesis experiments conducted by Peterson et al. it could be speculated that Phe1113 might be involved in the allosteric coupling of Ca²⁺ binding and DHP binding due to its close proximity to the Ca²⁺ binding Glu residue in the pore.⁴¹ Interestingly, in both models Tyr1508 residue is located in proximity of the EEEE locus, and really close to Phe1113 engaging with it charge transfer interactions. Taken together, these considerations strongly support the feasibility of the predicted adjustment of the P-loop on both

transmembrane bundle (a representation of the obtained adjustment of LCC P-loop in comparison with the KcsA one on the transmembrane bundle is given in figure 6). Subsequently, extensive energy minimization and molecular dynamics simulations were carried out on the both generated candidate models in order to investigate their stability and flexibility (see Computational Methods section).

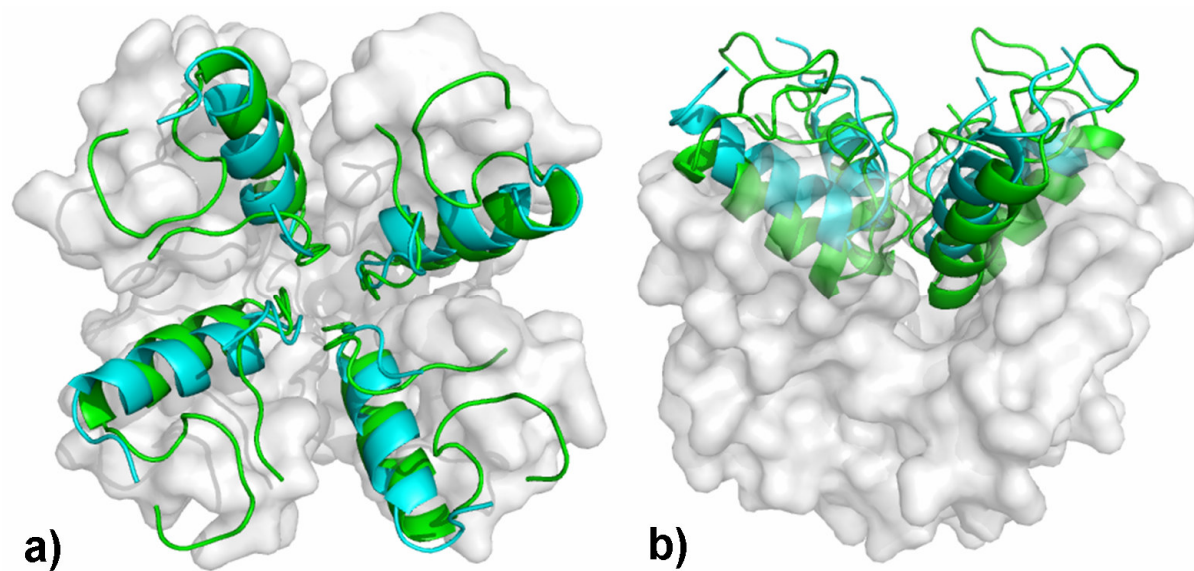


Figure 6. LCC model compared with the KcsA crystal structure. LCC transmembrane bundle is represented as a white transparent surface, LCC P-loop is represented as a cyan ribbon while KcsA loop region is represented as a green ribbon.

DHPs Docking

In order to shed light on the molecular basis of the interactions between LCC and its ligands, docking simulations were undertaken on several DHPs (chart 1) on both Model A and Model B. Such calculations were conducted employing the automated docking program AutoDock which has proven to be really effective in reproducing the experimentally found posing of ligands into their binding site.¹⁵ As shown in Table 2, the 50 independent docking runs performed for each ligand usually converged to a small number of different clusters (“clusters” of results differing by less than 1.5 Å rmsd). Generally, the top clusters (i.e. those with the most favourable ΔG_{bind}) were also associated with the highest frequency of occurrence, which suggests a good convergence behaviour of the search algorithm.

Even if the predicted free energy of binding can be used as tool for the choice of the best solution between the different alternative binding positions given by the docking software, in this case, the preference for one of them was also governed by its consistency with structure-activity relationships

(SARs) and mutagenesis data present in literature. In the following section a brief description of the calculated binding modes of the selected DHPs into both Model A and B is given.

Table 2. Result of 50 Independent Docking Runs for Each DHP^a

LCC Model	Ligand	N_{tot}	f_{occ}	ΔG_{bind}	Surrounding Residues
A	Nifedipine	7	23	-8.33	
	(<i>S</i>)-Nitrendipine	10	19	-7.94	
	(<i>S</i>)-Isradipine	9	17	-7.65	Gln1060 (IIS5), Phe1061 (IIS5), Ala1064 (IIS5), Phe1128 (IIP), Ser1131 (IIP), Thr1132 (IIP), Phe1133 (IIP), Tyr1169 (IIS6), Ile1170 (IIS6), Ile1172 (IIS6), Ile1173 (IIS6), Ala1174 (IIS6), Phe1176 (IIS6), Met1177 (IIS6),
	(<i>R</i>)-Amlodipine	20	14	-8.07	Met1178 (IIS6), Ile1180 (IIS6), Ile1505 (IVS6), Tyr1508 (IVS6), Met1509 (IVS6), Ala1512 (IVS6), Phe1513 (IVS6)
	Lacidipine	20	18	-8.12	
	(<i>S,S</i>)-Furnidipine	10	18	-9.49	
	(<i>S,S</i>)-Benidipine	23	13	-9.93	
	(<i>R</i>)-Benidipine	9	15	-8.74	
(<i>S</i>)-Bay K 8644	13	10	-7.43		
B	Nifedipine	5	18	-7.21	Gln1060 (IIS5), Phe1061 (IIS5), Phe1063 (IIS5), Ala1064 (IIS5), Cys1065 (IIS5), Leu1127 (IIP), Phe1128 (IIP), Thr1129 (IIP), Val1130 (IIP), Ser1131 (IIP), Thr1132 (IIP), Phe1133 (IIP), Ile1168 (IIS6), Tyr1169 (IIS6), Ile1170 (IIS6), Ile1171 (IIS6), Ile1172 (IIS6), Ile1173 (IIS6), Ala1174 (IIS6), Phe1175 (IIS6), Phe1176 (IIS6), Met1177 (IIS6), Phe1504 (IVS6), Ile1505 (IVS6), Ser1506 (IVS6), Phe1507 (IVS6), Tyr1508 (IVS6), Met1509 (IVS6), Leu1510 (IVS6), Ala1512 (IVS6), Phe1513 (IVS6), Thr1056 (IVS6), Thr1057 (IVS6)
	(<i>S</i>)-Nitrendipine	8	15	-7.18	
	(<i>S</i>)-Isradipine	6	27	-7.44	
	(<i>R</i>)-Amlodipine	24	10	-7.05	
	Lacidipine	14	13	-7.00	
	(<i>S,S</i>)-Furnidipine	11	21	8.22	
	(<i>S,S</i>)-Benidipine	22	14	-8.77	

^a N_{tot} is the total number of clusters; the number of results in the top cluster is given by the frequency of occurrence, f_{occ} ; ΔG_{bind} is the estimated free energy of binding for the top cluster results and is given in kcal/mol. The last column shows the contacting residues for the binding mode of the best cluster solution calculated (*S,S*)-benidipine. Only residues located within 5 Å from any atom of the docked ligand are reported. Residues reported to influence DHP binding are highlighted in bold.

DHPs Docking on Model A of LCC

Docking of nifedipine, nitrendipine, (*S*)-isradipine, (*R*)-amlodipine, lacidipine, (*S*)-furnidipine and (*S,S*)-benidipine into candidate A gave comparable binding solutions with the dihydropyridine ring fitting in the cleft formed by III S6, III S5, and IV S6 segments. Moreover in each docking calculation the best solution (in the present case the most consistent with SARs and mutagenesis data): i) the plane of the DHP ring is parallel to the pore axis, ii) the ligand NH group faces the III S5 segment, iii) the starboard side of the heterocyclic ring points upwards, iv) the plane of the 4-aryl substituent is perpendicular to the pore axis (Figure 7).

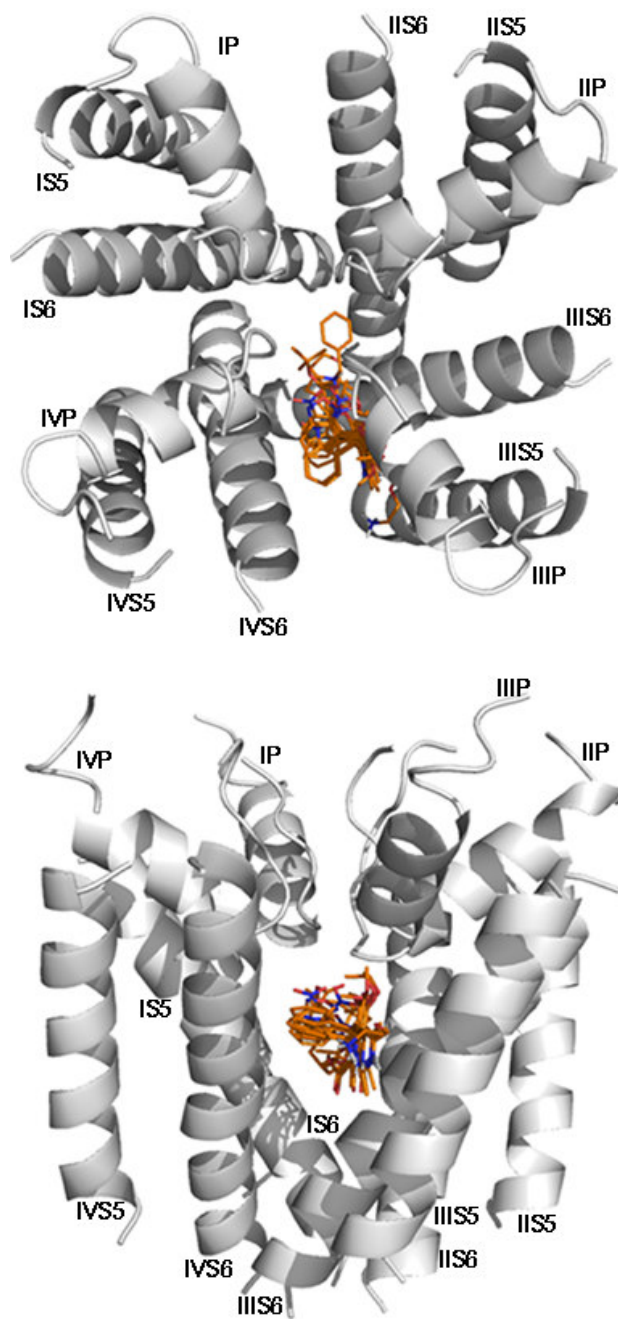


Figure 7. Top and side view of docked DHPs in model A of LCC. Ligands are represented as orange sticks while LCC is represented as grey ribbons

This orientation allows the molecules to establish several favourable contacts with the channel residues and the great majority these interactions revealed to be rather recurrent in the calculated posing of the inspected DHPs into the LCC binding site.

In all inspected ligands the N1 hydrogen atom of the heterocyclic ring H-bonds with the carbonyl oxygen of Gln1060 side-chain in III5 (Figure 8). This is in accordance with both SARs and mutagenesis data. In fact, SARs studies indicate that the N1 hydrogen atom has a key role in the binding of DHPs to LCC.¹⁷ Moreover, a mutational analysis by Mitterdorfer et al. clearly demonstrated that Gln1070 contributes to the binding of DHPs.³⁷ Interestingly, in the same study it was reported that mutation of Gln1070 to Asp did not affect the binding of DHPs indicating the participation of the glutamine side chain as H-bond acceptor in consonance with the proposed binding mode.

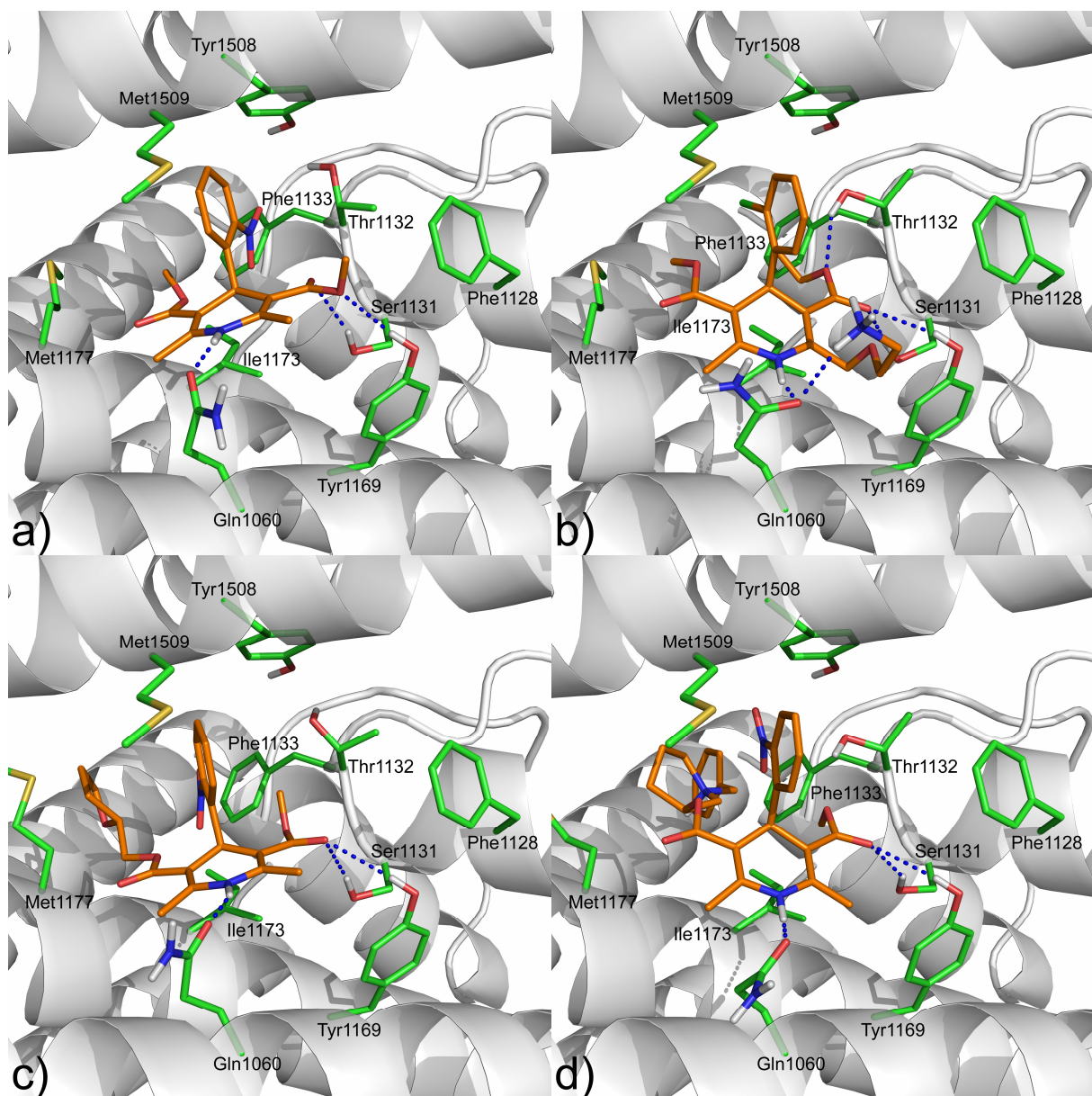


Figure 8. Docked structures of nifedipine (a), (*R*)-amlodipine (b), (*S,S*)-furnidipine (c) and (*S,S*)-benidipine in Model A of LCC. DHPs are displayed as white sticks, and key binding site residues are shown in green. Hydrogen bonds as represented with dashed blue lines.

As depicted in Figure 8, both the carbonyl and ester oxygens on the starboard side of the dihydropyridine ring form two H-bonds with the Ser1131 and Tyr1169 side chains. This is in accordance with SARs data indicating the involvement of this group in H-bond interactions with the channel.^{6,17} Moreover, it is also worth noting that the same study indicated that also the size of the ester group is important.¹⁷ Generally only small sized ester groups are tolerated on the starboard side of the DHP ring. This data might be rationalized by the fact that the above cited group adapts itself in a rather small cleft formed by Tyr1169, Phe1128, Thr1129, Ser1131 and Thr1132. Nevertheless, the location of the starboard side ester in this small cleft permits the establishing of favourable hydrophobic interactions between the methyl or the ethyl group on the DHP ester and Phe1128 side chain which has been reported to participate to the binding of DHPs.⁵⁰ The involvement of Tyr1169 in a H-bond with the carbonyl oxygen of the starboard side esters of (*R*)-amlodipine, (*S,S*)-benidipine and (*S,S*)-furnidipine and with the ester oxygen of the same group in nifedipine, (*S*)-isradipine, lacidipine and (*S*)-nitrendipine (see figure 8) is also in agreement with mutagenesis data. In fact, when mutating Tyr1169 to Ala (*S*)-isradipine

resulted to be 25 folds less active on the resulting mutant.⁴¹ Moreover, when Tyr1169 was mutated to Phe (*S*)-isradipine demonstrated to be 12.4 folds less active on the resulting mutant if compared with the wild type channel.⁴¹ This demonstrates the involvement of Tyr1169 hydroxyl group in a H-bond with the ligand in agreement with the proposed binding pose. The involvement of Ser1131 in the binding of DHPs was demonstrated by Yamaguchi et al. who reported that when mutating Ser1131 to Ala the IC₅₀ value of (*S*)-nitrendipine was 39.4 times higher than that of rbCII (rat brain Ca²⁺ channel α 1C subunit type II).⁵⁰

The 4-aryl substituent of the docked DHPs is in close contacts with Tyr1508 engaging with this residue a T-shaped charge transfer interaction. Also in this case the involvement of Tyr1508 in the binding of LCC DHPs antagonists was experimentally proven by mutagenesis studies. In fact, replacement of this residue to Ala has large effects on DHP activity with the K_D for DHP binding in Tyr1508Ala mutant increased by 6.1 folds.³⁸ Extensive SARs studies have unambiguously demonstrated that electron-withdrawing substituents in the 4-phenyl ring enhance activity in the *ortho*

and *meta* positions while any substituent in the *para* position is detrimental.^{6,17} This data can be rationalized by the proposed posing in fact a substituent in *para* position to the phenyl ring would give unfavourable steric clashes with the backbone atoms of Tyr1508 and Met1509 while substituents in both *ortho* and *meta* positions have enough space in the binding pocket.

The ester group on the port side of the DHP ring adopts a *cis* conformation to the double bond of the heterocyclic ring. The *trans* conformation does not appear to be feasible due to the unfavourable steric clashes that the large port side esters would give with IIS6 segment. Indeed, synthesis of DHP derivatives with an immobilized ester groups demonstrated the preference for a *cis* conformation of the port side ester. It is worth noting that the large lipophilic substituents on the port side ester establish favourable hydrophobic interactions with Met1177 and Met1178 which have been shown to participate to the binding of DHPs.⁴¹ Alternatively, the same substituent points towards the centre of the pore, establishing π - π charge transfer interactions with Phe1133 as in case of (*S,S*)-benidipine. Noticeably, lacidipine has a small port side ester although in this case the large lipophilic

substituent present in *ortho* on 4-phenyl ring occupies the same region of the above cited groups.

The entire DHP ring adapt itself on Ile1173 side-chain establishing with it favourable hydrophobic interactions. This data also agrees with mutagenesis studies indicating that mutation of Ile1173 to Ala results in a loss of potency on DHPs of 17 folds.

As regards positions 2 and 6 of the DHP ring, the majority of the analyzed drugs are characterized by the presence of methyl substituents. The only exception is found in (*R*)-amlodipine (Figure 8b) in which the flexible aminoethoxymethyl group through its protonated amine atom H-bonds with Gln1060 side chain carbonyl oxygen.

DHPs Docking on Model B of LCC

The binding orientation of the docked DHPs into model B of LCC roughly resembles one found for model A. In fact, as calculated by AutoDock, the DHP ring locates itself in the fissure between segments IIS6, IIS5 and IVS6 with the heterocyclic ring adapted in the same orientation found in model A with respect to the pore axis. If compared with results of DHPs docking on Model A, AutoDock was able to find basically the same sort of interactions when docking was performed on Model B of LCC. In fact, i) the N1 hydrogen atom of the DHP ring H-bonds with the carbonyl oxygen of Gln1060 side chain, ii) the carbonyl oxygen of the starboard side ester H-bonds with the hydroxyl group of Ser1131 side chain, iii) the ester on the port side of the DHP ring is favourably positioned in a *cis* orientation to the ring double bond so to allow the large ester portion to point towards the centre of the channel pore (Figure 9). This orientation permits the establishing of favourable hydrophobic interactions with Ile1173 and Met1177 which were reported to influence the DHP binding.⁴¹

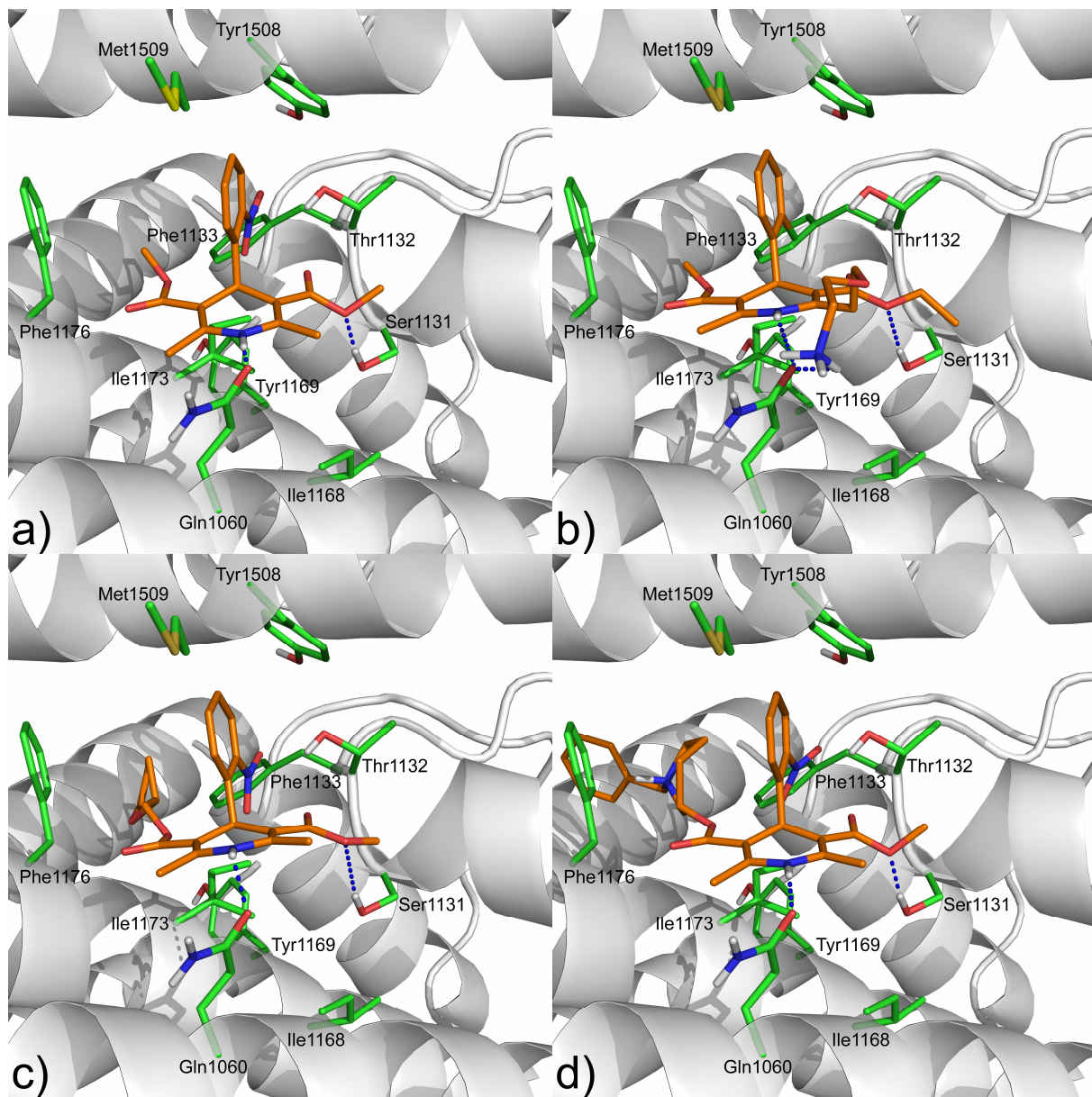


Figure 9. Docked structures of nifedipine (a), (*R*)-amlodipine (b), (*S,S*)-furnidipine (c) and (*S,S*)-benidipine in Model B of LCC. DHPs are displayed as white sticks, and key binding site residues are shown in green. Hydrogen bonds as represented with dashed blue lines.

Indeed, the different alignment of the IIS6 portion implicates the presence of different interactions with this segment. The most striking difference in the DHP binding to Model B of LCC resides in the absence of any interaction between the ligand and Tyr1169 which, as already mentioned, plays a crucial role in the recognition mechanism of DHP to LCC.⁴¹ Additionally in Model B, apart from Ile1173, the essential residues Met1177, Met1178 and Met1175 are placed far away from the docked DHPs.

From this point of view, the present calculations strongly indicate that the sequence alignment between IIS6 of LCC and M2 of KcsA in Model B could be unable to produce all the essential interactions with the DHP ring in the calculated binding pose. In this respect, the sequence alignment of IIS6 in Model A appears to be more in accordance with experimental findings such as SARS and mutagenesis data. Actually, the presence of two alternative sequence alignments was also reported in a previous paper by Lipkind et al. who gave the preference to candidate B rather than the A one.¹⁰ This decision was in the end dictated by correspondence between the proposed DHP binding mode in LCC and mutagenesis data. In fact, in this study nifedipine, (-)-Bay K8644 (LCC agonist), a derivative of nifedipine

with an isopropyl ester group on the port side and a DHP with fused thiophene ring were manually docked into LCC. Possibly, it could be hypothesized that manual docking exercises always require some subjective decisions, and there is the danger that personal biases, ambiguous experimental data, or misinterpretation of experimental results could corrupt the manual ligand-docking exercises. On the contrary, in the present study docking calculation of DHPs into LCC were all performed employing an automated docking software such as AutoDock. Hence, discrepancies between the sequence alignment suggested by Lipkind et al. and the one proposed herein could have arisen due to the different docking approaches adopted.

From Antagonist to Agonist DHPs

In this theoretical study a peculiar pharmacological behaviour of some DHPs was also rationalized. In fact, it is well known that some of these compounds exhibit an interesting stereoselective duality of action, with one enantiomer behaving as an agonist and the other one having antagonist properties. Indeed, these LCC activators do not have any therapeutic role, nevertheless they represent one of the incongruities of the medicinal chemistry. For these reasons, both the antagonist (*R*)-enantiomer and the agonist (*S*)-enantiomer of Bay K 8644⁵² were also docked.

As expected, the predicted posing of (*R*)-Bay K 8644 into Model A of LCC strongly resembles the previously described ones establishing the same polar and hydrophobic interactions found for the previously mentioned antagonists (Figure 10a). It is worth noting that the vicinity of the ligand port side ester with the hydrophobic residues at the crevice between the of IIS6 and IVS6 segments could impede the conformational rearrangements of these segments thus stabilizing the inactivated state of the channel.⁴² In fact,

it is well known that voltage-gated channels seem to open by movement of the inner parts of the S6 α -helices.⁵³

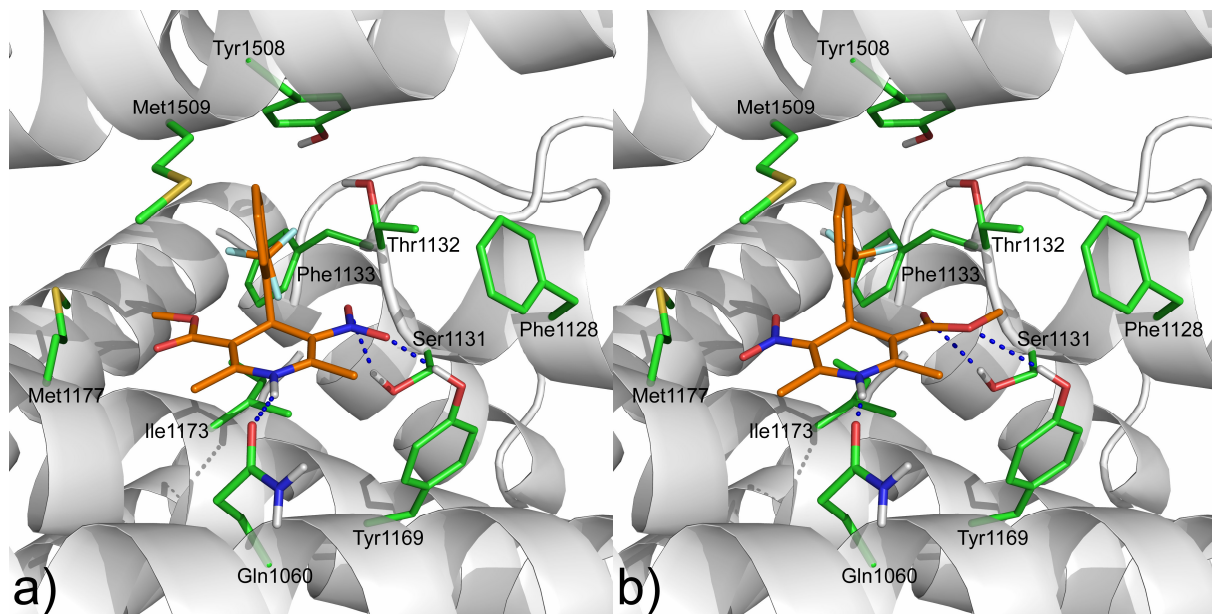


Figure 10. Docked structures of (*R*)-Bay K 8644 (a) and (*S*)-Bay K 8644 (b) in Model A of LCC. DHPs are displayed as white sticks, and key binding site residues are shown in green. Hydrogen bonds as represented with dashed blue lines

Also for the (*S*)-enantiomer of Bay K 8644 the calculated posing was pretty similar with what already found for the (*R*)-one and this is in accordance with experimental data suggesting that both DHP agonist and antagonists should share the same binding site.⁴² Obviously, the different absolute configuration of the chiral centre in position 4 allows different interactions with LCC. In fact, in this case the nitro group on the port side faces the bottom of the channel pore while the starboard side points outwards H-bonding with Ser1131 and Tyr1169 (Figure 10b). The main differences in the calculated binding mode of (*S*)-Bay K 8644 with respect to the (*R*)-one mainly resides in the absence of any interaction with the hydrophobic residues present at the intersection between the III and IVS6 segments in which the main structural rearrangement occur during the channel opening. Therefore, the lack of such an interaction could explain the reasons for the absence of any antagonist activity of this enantiomer towards. Moreover, the latter ligand exposes his hydrophilic nitro group to an hydrophobic surface at the junction of the S6 segments of repeat III and IV in the closed state, making such an interaction energetically unfavourable. Therefore, it could be hypothesized that the agonist could destabilize the closed state of LCC and

could stabilize the opened one. Further studies should be undertaken to elucidate the conformation of the channel in the open state and then use it to dock the agonist ligands eventually confirming such an hypothesis.

CONCLUSIONS

In this contribution results of a computational study on the human cardiac L-Type Ca^{2+} channel which is one of the most important biological targets of pharmaceutical interest are reported. A 3D model of this channel was built using the crystallographic structure of KcsA as a template considered to be a predecessor of the six-transmembrane segment ion channels. Extensive mutagenesis data present in literature LCC allowed to perform a pairwise alignment between the sequences of the two proteins leading to two different arrangements which were used to construct two candidate models of LCC (Model A and B). After construction of the transmembrane bundle and P-loop region of LCC alone, the latter was adapted on the intracellular portion through rigid-body protein-protein docking calculations. Both Model A and B were then comprehensively validated employing MD simulations.

Automated docking simulations were then conducted using both Model A and B on nine different DHP antagonists featuring molecular diversity. These calculations allowed to detect the presence of a similar posing in both theoretical models in which: the plane of the DHP ring is parallel to the pore axis, the ligand NH group faces the IIS5 segment, the starboard side of the heterocyclic ring points upwards and the plane of the 4-aryl substituent is

perpendicular to the pore axis (Figure 7). Despite the comparable binding orientation of DHPs antagonists in both candidates, dissimilar interaction patterns were detected between ligands and LCC with the most prominent difference residing in the lack of specific interactions with the IIS6 segment in Model B. In particular, in this structure the ligand is unable to interact with Tyr1169 residue which was reported to have a key role in the interaction with DHP antagonists.⁴¹ In this respect, the coherence between docking results obtained with structure A and SARs and mutagenesis data would drive the preference towards this candidate rather than the B one. In fact the correlation between the predicted binding pose in Model A and the large body of evidence regarding mutagenesis information for the protein and SARs data for ligands demonstrated that this model is very realistic and reveals an insight into the binding pose of DHPs antagonists. In particular, these drugs fit into LCC binding site adopting a sort of “spider” conformation (seer Figure 8) with the DHP ring resembling the body of the animal and the substituents in position 2, 3, 5 and 6 resembling the legs. This arrangement allows the formation of several H-bond interactions with LCC through their NH group with the carbonyl oxygen of Gln1060 side-chain and

through their starboard side ester oxygens with Ser1131 and Tyr1169 side chains. Moreover, the same ester points in a rather small cleft formed by Tyr1169, Phe1128, Thr1129, Ser1131 and Thr1132. The 4-aryl substituent of the docked DHPs is in close contacts with Tyr1508 engaging with this residue a T-shaped charge transfer interaction and the adjacent port side ester group, adopting a *cis* conformation, points towards the centre of the pore establishing favourable hydrophobic interactions with Met1177, Met1178 and Phe1133. Additional hydrophobic interactions are also engaged by the entire DHP ring and Ile1173 side chain.

The described posing of DHP antagonist into LCC inner pore might also help in suggesting a possible mechanism of action. In fact, LCC is believed to open through a movement of the C-terminal part of S6 segments of each repeat resulting in a widening of this region that allows the passage of Ca²⁺ ions.⁵³ In the predicted binding pose of the selected DHPs the port side ester establishes favourable hydrophobic interactions with the lipophilic C-terminal residues of IIS6 and IVS6 segments. Therefore, it might be speculated that such an interaction might stabilize the inactivated state of

LCC by preventing the relocation of IIIS6 and IVS6 segments required for the opening of the channel.

In conclusion, herein a molecular modeling study aimed at providing both a structural model of LCC central pore and a detailed description of the posing of DHPs antagonists into the channel binding site has been presented. Such model provided plausible hypotheses for ligand-channel interactions satisfactorily explaining the large body of SARs data available in literature and revealing the key residues that interact with ligands. Further studies in this direction would validate this model, which could subsequently be used for de novo drug design. It is worth noting that the validity of this theoretical model relies on some assumptions and remains speculative. However, the coherence of many observations on the 3D models might not be fortuitous. Furthermore, only the central pore of LCC was constructed and a complete model of the channel α_1 subunit would also require inclusion of additional helix per repeat, for which no structural template exists. Though, none of these issues is insurmountable.⁵⁴

REFERENCES

1. Heilbrunn, L. V. *An Outline of General Physiology*. Eds. 1, 2, 3. Philadelphia, W. B. Saunders Co. 1937-1943. (b) Carafoli, E. Calcium signaling: a tale for all seasons. *Proc. Natl. Acad. Sci. USA* **2002**, *99*, 1115-1122. (c) Berridge, M. J.; Lipp, P.; Bootman, M. D. The versatility and universality of calcium signaling. *Nat. Rev. Mol. Biol.* **2000**, *1*, 11-21. (d) Verkhatsky, A.; Landfield, P. W.; Thibault, O. Ca²⁺ and neuronal pathology. *Eur. J. Pharmacol.* **2002**, *447*, 115-296.
2. Birnbaumer, L.; Campbell, K. P.; Catterall, W. A.; Harpold, M. M.; Hofmann, F.; Horne, W. A.; Mori, Y.; Schwartz, A.; Snutch, T. P.; Tanabe, T.; Tsien, R. W. The naming of voltage-gated calcium channels. *Neuron* **1994**, *13*, 505-506. (b) Catterall, W. A. Structure and function of voltage-gated ion channels. *Annu Rev Biochem.* **1995**, *64*, 493-531. (c) Hofmann, F.; Biel, M.; Flockerzi, V. Molecular basis for Ca²⁺ channel diversity. *Annu. Rev. Neurosci.* **1994**, *17*, 399-418.

3. Catterall W. A; Striessnig, J.; Snutch, T. P.; Perez-Reyes, E. International Union of Pharmacology. XL. Compendium of voltage-gated ion channels. Calcium channels. *Pharmacol. Revs.* **2003**, *55*, 579-581. (b) Catterall W. A; Perez-Reyes, E.; Terrance, P.; Striessnig, J. International Union of Pharmacology. XLVIII. Nomenclature and structure-function relationships of voltage-gated calcium channels. *Pharmacol. Revs.* **2005**, *57*, 411-425.
4. Hille, B. *Ionic Channels of Excitable Membranes* **2001**, 3rd Ed, Sinauer, Sunderland,MA
5. Hille, B. *Ionic Channels of Excitable Membranes* **1992**, 2nd ed., Sinauer, Sunderland, MA.
6. Triggle, D. J.; Rampe, D. 1,4-Dihydropyridine activators and antagonists: structural and functional distinctions. *Trends Pharmacol. Sci.* **1989**, *10*, 507-511. (b) Triggle, D. J. Calcium, calcium channels, and calcium channel antagonists. *Can. J. Physiol. Pharmacol.* **1990**, *68*, 1474-1481. (c) Triggle, D. J. Calcium-channel drugs: structure-

function relationships and selectivity of action. *J. Cardiovasc. Pharmacol.* **1991**, *18*, S1-S6. (d) Triggle, D. J. Sites, mechanisms of action, and differentiation of calcium channel antagonists. *Am. J. Hypertension* **1991**, *4*, 422S-429S. (e) Triggle, D. J. Molecular pharmacology of voltage-gated calcium channels. *Ann. N.Y. Acad. Sci.* **1994**, *15*, 267-281. (f) Triggle, D. J. Ion channels as pharmacologic receptors: the chirality of drug interactions. *Chirality* **1996**, *8*, 35-38. (g) Triggle DJ. L-type calcium channels. *Curr. Pharm. Des.* **2006**, *12*, 443-457.

7. Catterall, W. A.; Striessnig, J. Receptor sites for Ca²⁺ channel antagonists. *Trends Pharmacol. Sci.* **1992**, *13*, 256-262.
8. Glossmann, H.; Ferry, D. R.; Goll, A.; Rombusch, M. Molecular pharmacology of the calcium channel: evidence for subtypes, multiple drug-receptor sites, channel subunits, and the development of a radioiodinated 1,4-dihydropyridine calcium channel label, [125I]iodipine. *J. Cardiovasc. Pharmacol.* **1984**, *6*, 508-621.

9. Peterson B. Z.; Catterall, W. A. Calcium binding in the pore of L-type calcium channels modulates high affinity dihydropyridine binding. *J. Biol. Chem.* **1995**, *270*, 18201–18204.
10. Lipkind, G. M.; Fozzard, H. A. Molecular modeling of the interaction of dihydropyridines and phenylalkylamines with the inner pore of the L-type Ca²⁺ channel. *Mol. Pharmacol.* **2003**, *63*, 499-511.
11. Zhorov, B. S.; Folkman, E. V.; Ananthanarayanan, V. S. Homology model of dihydropyridine receptor: implications for L-type Ca²⁺ channel modulation by agonists and antagonists. *Arch Biochem Biophys.* **2001**, *393*, 22-41.
12. Doyle, D. A.; Cabral, J. M.; Pfuetzner, R. A.; Kuo, A.; Gulbis, J. M.; Cohen, S. L.; Chait, B. T.; MacKinnon, R. The structure of the potassium channel: molecular basis of K⁺ conduction and selectivity. *Science* **1998**, *280*, 69-74.

13. Zhorov, B. S.; Tikhonov, D. B. Potassium, sodium, calcium and glutamate-gated channels: pore architecture and ligand action. *J Neurochem.* **2004**, *88*, 782-799.
14. Jiang, Y.; Lee, A.; Chen, J.; Cadene, M.; Chait, B. T.; MacKinnon, R. Crystal structure and mechanism of a calcium-gated potassium channel. *Nature* **2002**, *417*, 515-522.
15. Morris, G. M.; Goodsell, D. S.; Halliday, R. S.; Huey, R.; Hart, W. E.; Belew, R. K.; Olson, A. J. Automated docking using a Lamarckian genetic algorithm and an empirical binding free energy function. *J. Comput. Chem.* **1998**, *19*, 1639-1662. (The Scripps Research Institute, La Jolla, CA 92037-1000).
16. Goodsell, D. S.; Morris, G. M.; Olson, A. J. Automated docking of flexible ligands: Applications of AutoDock. *J. Mol. Recognit.* **1996**, *9*, 1-5.

17. Goldmann, S.; Stoltefuss, J. 1,4-Dihydropyridines: effects of chirality and conformation on the calcium antagonist and calcium agonist activities. *Angew. Chem. Int. Ed. Engl.* **1991**, *30*, 1559-1578.
18. Bossert, F.; Vater, W. U.S. Patent 3,485,847, Dec 23, 1969. (b) Vater, W.; Kroneberg, G.; Hoffmeister, F.; Saller, H.; Meng, K.; Oberdorf, A.; Puls, W.; Schlossmann, K.; Stoepel, K. Pharmacology of 4-(2'-nitrophenyl)-2,6-dimethyl-1,4-dihydropyridine-3,5-dicarboxylic acid dimethyl ester (Nifedipine, BAY a 1040). *Arzneimittelforschung* **1972**, *22*, 1-14.
19. Stoepel, A.; Heise, S.; Kazda, S. Pharmacological studies of the antihypertensive effect of nitrendipine. *Arzneimittelforschung* **1981**, *32*, 2056-2064; (b) Meyer, H.; Bossert, F.; Wehinger, E.; Stoepel, K.; Vater, W. Synthesis and comparative pharmacological studies of 1,4-dihydro-2,6-dimethyl-4-(3-nitrophenyl)pyridine-3,5-dicarboxylates with non-identical ester functions. *Arzneimittelforschung* **1981**, *31*, 407-409. (b) Mikus, G.; Mast, V.; Ratge, D.; Wisser, H.; Eichelbaum, M. Stereoselectivity in cardiovascular and biochemical action of

calcium antagonists: studies with the enantiomers of the dihydropyridine nitrendipine. *Clin Pharmacol Ther.* **1995**, *57*, 52-61.

20. Bristol, J. A., Ed. In *Annu. Rep. Med. Chem.* **1992**, *27*, 330.
21. Fitton, A.; Benfield, P. Isradipine. A review of its pharmacodynamic and pharmacokinetic properties, and therapeutic use in cardiovascular disease. *Drugs* **1990**, *40*, 31-74. (b) Hof, R. P.; Hof, A.; Ruegg, U. T.; Cook, N. S.; Vogel, A. Stereoselectivity at the calcium channel: different profiles of hemodynamic activity of the enantiomers of the dihydropyridine derivative PN 200-110. *J Cardiovasc Pharmacol.* **1986**, *8*, 221-226.
22. Arrowsmith, J. E.; Campbell, S. F.; Cross, P. E.; Stubbs, J. K.; Burges, R. A.; Gardiner, D. G.; Blackburn, K. J. Long-acting dihydropyridine calcium antagonists. 1. 2-Alkoxyethyl derivatives incorporating basic substituents. *J. Med. Chem.* **1986**, *29*, 1696-1702.
23. (a) Alajarin, R.; Vaquero, J. J.; Alvarez-Builla, J.; Pastor, M.; Sunkel, C.; de Casa-Juana, M. F.; Priego, J.; Statkow, P. R.; Sanz-Aparicio, J.

Synthesis and chromatographic separation of the stereoisomers of furnidipine. *Tetrahedron: Asymmetry* **1993**, 4, 617-620. (b) Alajarin, R.; Alvarez-Builla, J.; Vaquero, J. J.; Sunkel, C.; de Casa-Juana, M. F.; Statkow, P. R.; Sanz-Aparicio, J.; Fonseka, I. Synthesis, structure, and pharmacological evaluation of the stereoisomers of furnidipine. *J. Med. Chem.* **1995**, 38, 2830-2841.

24. Ishii, A.; Nishida, K.; Oka, T.; Nakamizo, N. Receptor binding properties of the new calcium antagonist benidipine hydrochloride. *Arzneimittelforschung* **1988**, 38, 1677-1680.
25. SYBYL Molecular Modelling System, version 6.9.1; Tripos Inc.: St. Louis, MO, 2003.
26. Accelrys Inc., San Diego, CA., (b) Accelrys Inc. *DiscoVer3*; 2.98 ed.: San Diego, CA.
27. DISCOVER, Version 95.0; BIOSYM Technologies, 10065 Barnes Canyon Rd, San Diego, CA 92121. (b) Hagler, A. F.; Lifson, S.;

- Dauber, P. Consistent force field studies of intermolecular forces in hydrogen-bonded crystals. *J. Am. Chem. Soc.* **1979**, *101*, 5122-5130.
28. Bairoch, A.; Apweiler, R. The SWISS-PROT protein sequence database and its supplement TrEMBL in 2000. *Nucleic Acids Res.* **2000**, *28*, 45-48.
29. Chen, R.; Li, L.; Weng, Z. ZDOCK: An initial-stage protein docking algorithm. *Proteins* **2003**, *52*, 80–87.
30. Katchalski-Katzir, E.; Shariv, I.; Eisenstein, M.; Friesem, A.; Aflalo, C.; Vakser, I. A. Molecular surface recognition-determination of geometric fit between proteins and their ligands by correlation techniques. *Proc. Natl. Acad. Sci. USA* **1992**, *89*, 2195-2199.
31. Zhang, C; Vasmatzis, G; Cornette, J. L.; DeLisi, C. Determination of atomic desolvation energies from the structures of crystallized proteins. *J. Mol. Biol.* **1997**, *267*, 707-726.
32. Comeau, S. R.; Gatchell, D. W.; Vajda, S.; Camacho, C. J. ClusPro: an automated docking and discrimination method for the prediction

- of protein complexes. *Bioinformatics* **2004**, *20*, 45-50. (b) Comeau R.; Gatchell, D. W.; Vajda, S.; Camacho, C. J. ClusPro: a fully automated algorithm for protein-protein docking. *Nucl. Acids Res.* **2004**, *32*, W96-99.
33. Laskowski, R. A.; MacArthur, M. W.; Moss, D. S.; Thornton, J. M. PROCHECK: a Program to Check the Stereochemical Quality of Protein Structures. *J. Appl. Crystallogr.* **1993**, *26*, 283-291.
34. Allen, F. H.; Bellard, S.; Brice, M. D.; Cartwright, B. A.; Doubleday, A.; Higgs, H.; Hummelink, T.; Hummelink-Peters, B. G.; Kennard, O.; Motherwell, W. D. S. The Cambridge crystallographic data center: Computer-based search, retrieval, analysis and display of information. *Acta Crystallogr.* **1979**, *B35*, 2331-2339.
35. Head, J.; Zerner, M. C. A Broyden-Fletcher-Goldfarb-Shannon optimization procedure for molecular geometries. *Chem. Phys. Lett.* **1985**, *122*, 264-274.

36. Gasteiger, J.; Marsili, M. Iterative partial equilization of orbital electronegativys. A rapid access to atomic charges. *Tetrahedron* **1980**, *36*, 3219-3228.
37. Hockerman, G. H.; Johnson, B. D.; Scheuer, T.; Catterall, W. A. Molecular determinants of high-affinity phenylalkylamine block of L-type calcium channels. *J. Biol. Chem.* **1995**, *270*, 22119-22122.
38. (a) Mitterdorfer, J.; Wang, Z.; Sinnegger, M. J.; Hering, S.; Striessnig, J. Grabner, M.; Glossmann, H. Two amino acid residues in the IIIIS5 segment of L-type calcium channels differentially contribute to 1,4-dihydropyridine sensitivity. *J. Biol. Chem.* **1996**, *271*, 30330-30335.
- (b) Mitterdorfer, J.; Wang, Z.; Sinnegger, M. J.; Hering, S.; Striessnig, J.; Grabner, M.; Glossmann, H. Two amino acid residues in the IIIIS5 segment of L-type calcium channels differentially contribute to 1,4-dihydropyridine sensitivity. *J. Biol. Chem.* **1996**, *271*, 30330-30335.

39. Grabner, M.; Wang, Z.; Hering, S.; Striessnig, J.; Glossmann, H.
Transfer of 1,4-dihydropyridine sensitivity from L-type to class
A(B1) calcium channels. *Neuron* **1996**, *16*, 207-218.
40. Schuster, A.; Lacinova, L.; Klugbauer, N.; Ito, H.; Birnbaumer, L.;
Hofmann, F. The IVS6 segment of the L-type calcium channel is
critical for the action of dihydropyridines and phenylalkylamines.
EMBO J. **1996**, *15*, 2365-2370.
41. Peterson, B. Z.; Johnson, B. D.; Hockerman, G. H.; Acheson, M.;
Scheuer, T.; Catterall, W. A. Analysis of the dihydropyridine receptor
site of L-type calcium channels by alanine-scanning mutagenesis. *J.*
Biol. Chem. **1997**, *272*, 18752-18758.
42. Hockerman, G. H.; Peterson, B. Z.; Johnson, B. D.; Catterall, W. A.
Molecular determinants of drug binding and action of L-type calcium
channels. *Annu. Rev. Pharmacol. Toxicol.* **1997**, *37*, 361-396.

43. He, M.; Bodi, I.; Mikala, G.; Schwartz, A. Motif IIIIS5 of L-type calcium channels involved in the dihydropyridine binding site. *J. Biol. Chem.* **1997**, *271*, 2629-2633.
44. Lipkind, G. M.; Fozzard, H. A. Modeling of the outer vestibule and selectivity filter of the L-type Ca²⁺ Channel. *Biochemistry* **2001**, *40*, 6786-6794
45. Tikhonov, D. B.; Zhorov, B. S. Modeling P-loops domain of sodium channel: homology with potassium channels and interaction with ligands. *Biophys. J.* **2005**, *88*, 184-197.
46. Heinemann, S. M.; Terlau, H.; Stuhmer, W.; Imoto, W.; Numa, S. Calcium channel characteristics conferred on the sodium channel by single mutations. *Nature* **1992**, *356*, 441-443.
47. Hess, P.; Tsien, R. W. Mechanism of ion permeation through calcium channels. *Nature* **1984**, *309*, 453-456.
48. Tang, S.; Mikala, G.; Bahinski, A.; Yatani, A.; Varadi, G., Schwartz, A. Molecular localization of ion selectivity sites within the pore of a

- human L-type cardiac calcium channel. *J. Biol. Chem.* **1993**, *268*, 13026-13029.
49. Yamaguchi, S.; Zhorov, B. S.; Yoshioka, K.; Nagao, T.; Ichijo, H.; Adachi-Akahane, S. Key roles of Phe1112 and Ser1115 in the pore-forming IIS5-S6 linker of L-type Ca^{2+} channel α -1C subunit (Cav1.2) in binding of dihydropyridines and action of Ca^{2+} channel agonists. *Mol. Pharmacol.* **2003**, *64*, 235-248.
50. Ellinor, P. T.; Yang, J.; Sather, W. A.; Zhang, J. F.; Tsien, R. W. Ca^{2+} channel selectivity at a single locus for high-affinity Ca^{2+} interactions. *Neuron* **1995**, *15*, 1121-1132.
51. Wiehe, K.; Pierce, B.; Mintseris, J.; Tong, W. W.; Anderson, R.; Chen, R.; Weng, Z. ZDOCK and RDOCK performance in CAPRI rounds 3, 4, and 5. *Proteins* **2005**, *60*, 207-213.
52. Schramm, M.; Thomas, G.; Towart, R.; Franckowiak, G. Activation of calcium channels by novel 1,4-dihydropyridines. A new

mechanism for positive inotropics or smooth muscle stimulants.

Arzneimittelforschung. **1983**, 33, 1268-72.

53. Liu, Y.; Holmgren, M.; Jurman, M. E; Yellen, G. Gated access to the pore of a voltage-dependent K⁺ channel. *Neuron* **1997**, 19,175–184.

54. Treptow, W.; Maigret, B.; Chipot, C.; Tarek, M. Coupled motions between pore and voltage-sensor domains: a model for Shaker B, a voltage-gated potassium channel. *Biophys. J.* **2004**, 87, 2365-2379.